Fermi National Accelerator Laboratory

FERMILAB-Pub-87/100-T
LBL-23504
June, 1987

Higgs decay to $\tau^+\tau^-$: A possible signature of intermediate mass Higgs bosons at the SSC.

R. K. Ellis
Fermi National Accelerator Laboratory
P. O. Box 500, Batavia, Illinois 60510
I. Hinchliffe*
Lawrence Berkeley Laboratory
Berkeley, California 94720.
M. Soldate and J.J. van der Bij
Fermi National Accelerator Laboratory
P. O. Box 500, Batavia, Illinois 60510

Abstract

This paper considers the decay of a standard model Higgs boson into a tau pair, as a possible signature at the SSC for a Higgs boson of mass between 110 and 160 GeV. The production of the Higgs in association with a large transverse momentum jet is considered, since this may aid in reconstructing the Higgs mass. The background from the production of tau pairs via virtual photons and Z's is shown not to be a serious problem. We comment on the possible use of this process to search for a light Higgs at the Tevatron collider.

---

*Work supported by the Director, Office of Energy Research, Office of High Energy Physics, Division of High Energy Physics of the U.S. Department of Energy under Contract DE-AC03-76SF00098.

I. INTRODUCTION

Only two particles of the standard model[1] remain to be found, the top quark and the Higgs boson. Of these the latter is the more important since it lies at the root of the symmetry breaking mechanism which generates the masses of the vector bosons (M_W and M_Z). Although the vacuum expectation value of the Higgs field is of order 250 GeV, the mass of the Higgs boson is only weakly constrained. Arguments concerning the stability of the Higgs potential[2] imply that its mass should be greater than 10 GeV provided that the top quark is not too heavy. On the other hand if the mass of the Higgs exceeds 1 TeV, it becomes strongly coupled to W's and Z's and no longer behaves as a particle.[3] In this scenario one must search for other manifestations of the weak symmetry breaking.[4]

A large number of mechanisms have been proposed to search for the Higgs boson.[5] If its mass is less than 40 GeV, it should be detectable via the decay $Z \rightarrow H\mu^+\mu^-$ at LEP or SLC.[6] Masses of up to 90 GeV should be reachable at LEP 200 via the process $e^+e^- \rightarrow Z + H$.[7] In addition an e^+e^- machine which is able to produce toponium should be able to see the decay into $H + \gamma$ which occurs with a branching ratio of order a few percent.[8] The accessible mass depends on the mass of toponium; if toponium exists with a mass of order 160 GeV, LEP 200 may be able to probe Higgs masses well above M_Z.

It is possible that the e^+e^- machines under construction do not have sufficient energy, perhaps because toponium does not exist with the right mass to exploit fully their potential to find the Higgs. In this case the Higgs boson must be looked for at the SSC. Searches for the Higgs boson at the SSC fall into two classes. If the Higgs boson mass is greater than $2M_W$ then it will decay dominantly into a W or Z pair. The cleanest channels involve the decay of the Z pair into leptons, and will enable a Higgs boson with mass up to 1 TeV to be found only if the full design luminosity of $10^{33} cm^{-2} sec^{-1}$ can be exploited.[9] The situation regarding the intermediate mass Higgs boson ($M_W < M_H < 2M_W$) is much more complicated. Both its production and decay properties depend upon the top quark mass.

If $M_H > 2m_t$, then the Higgs decays dominantly into $t\bar{t}$ final states. In this decay channel the inclusive Higgs signal is overwhelmed by the background from the QCD production of $t\bar{t}$ pairs.[10] The production of a Higgs in association with a W

has a smaller cross section but produces a final state where the signal to background ratio is potentially much better.[11] Unfortunately a detailed analysis indicates that an adequate determination of the invariant mass of the $t\bar{t}$ system is not possible.[12]

There is some indirect evidence which suggests that the top quark could be quite heavy[13], in which case it is important to consider the case that $M_H < 2m_t$. In this case the dominant decay channel is $b\bar{b}$. If M_H is close to $2M_W$ then the channel $H \to Wf\bar{f}$ can also become important[14] and must be included in the calculation of branching ratios. If the Higgs decays predominantly to bottom quarks, the associated production of the Higgs and a W may be observable[15] since the b quark jets are better defined than t quark jets. Nevertheless it is important that other channels be investigated.

One very clean channel is the decay to a pair of photons which occurs with a width of,[16]

$$\Gamma(H \to \gamma\gamma) = \frac{\alpha^2 \alpha_W M_H^3}{2^8 \pi^2 M_W^2} |F|^2 \tag{1.1}$$

with $F = F_W(\beta_W) + \sum_f F_f(\beta_f)$, $\beta_i = 4m_i^2/M_H^2$. The form factors F_i are given in ref. 16 and

$$\alpha_W = \frac{g_W^2}{4\pi} = \frac{e^2}{4\pi sin^2(\theta_W)} \ . \tag{1.2}$$

Eq.(1.1) implies a branching ratio of 7×10^{-4} for M_H of 100 GeV rising slowly to 10^{-3} at M_H of 150 GeV, assuming that the $t\bar{t}$ channel is closed. In this range the width is dominated by the contribution from the W loop which has a value close to its asymptotic value $F_W(\infty) = 7$. It is insensitive to values of the top quark mass in the range between 40 and 250 GeV.

In this paper we primarily consider the decay to a tau pair which occurs with a width of,

$$\Gamma(H \to \tau^+\tau^-) = \frac{\alpha_W m_\tau^2 M_H}{8M_W^2}\left(1 - \frac{4m_\tau^2}{M_H^2}\right)^{3/2} \ . \tag{1.3}$$

For Higgs masses of 110, 140 and 160 GeV and $M_W = 81$ GeV this implies a branching ratio of 3.5%, 2.2% and .5% respectively. The drop in the branching ratio at values of M_H close to $2M_W$ is caused by the decay to $Wf\bar{f}$.

For Higgs bosons in the mass range of interest the production is dominated by the gluon fusion process shown in Fig. 1. The rate is sensitive to the quark masses

appearing in the loop and is given by,[17]

$$\sigma = \frac{\alpha_W \alpha_S^2}{32V} \frac{M_H^2}{M_W^2} |A_1|^2 \ \delta(s - m_H^2) \tag{1.4}$$

where $V = N^2 - 1 = 8$ is the number of gluons in the adjoint representation of the $SU(N)$ colour group. A_1 is a function coming from the triangle diagram which contains the dependence on the mass of quarks in the internal loop. The exact expression for A_1 is given in the appendix. For a single flavour of very heavy internal fermion,

$$A_1(M_H^2) \to \frac{2}{3} \ . \tag{1.5}$$

Notice that in this limit the cross section in Eq.(1.4) is independent of m_f. The corresponding result for a very light quark is,

$$A_1(M_H^2) \to -\frac{m_f^2}{M_H^2} \log^2(m_f) \ . \tag{1.6}$$

Hence for very small m_f, the cross section is proportional to $m_f^2/M_H^2 \log^2 m_f$ if there is another heavier quark; if this is not the case then the contribution is proportional to $m_f^4/M_H^4 \log^4 m_f$.

The production rate from gluon fusion is shown in Fig. 2. Only the top quark contribution is included; contributions from other quarks are numerically insignificant. Since we are interested in the decay to a tau pair, the dominant background will arise from the production of a tau pair via an intermediate virtual photon or Z. The cross section $d\sigma/dm/dy$ for the production of a tau pair of mass m is shown in Fig. 3. It is clear from a comparison of these figures that the Higgs signal will be comparable to the background if (a) a resolution of order 10 GeV in the tau pair invariant mass can be achieved, and (b) the decay channel to $t\bar{t}$ pairs is closed and the branching ratio $H \to \tau^+\tau^-$ is as given above. If the Higgs can decay to $t\bar{t}$, the branching ratio to a tau pair is at most $m_\tau^2/3m_t^2 < 0.25\%$ and the signal will be completely obscured by the background. We will therefore only consider the case in which the Higgs can not decay to top quarks. Note also that if the Higgs mass is too close to the mass of the Z, the signal will be swamped by the background.

When a tau decays, it produces a final state with missing energy which is carried off by one or more neutrinos. If the masses of all particles involved in the decay of

the tau are small compared to their momenta, the direction of the tau is determined by the direction of its observed visible decay products.

When the transverse momentum of the Higgs is small the two taus are moving back to back. Accurate reconstruction of the individual transverse momenta of the two taus is not possible. The resolution in the tau pair invariant mass will be poor and the signal difficult to extract.

The situation may be improved if the Higgs is produced with large transverse momentum which is balanced by a hadronic jet. The transverse momentum of the tau pair can be determined from a measurement of the transverse momentum of the hadronic jet. Since we know the directions of the individual taus in the transverse plane, the transverse momentum of each tau can be obtained. Since we also know the direction of each of the taus, their three momenta can be fully reconstructed from their transverse momenta. In principle, therefore, much better resolution on the tau pair invariant mass can be obtained. In order to further assess the feasibility of the method we must calculate the production rate of Higgs bosons at large transverse momenta.

II. Higgs Bosons at Large Transverse Momenta

At order α_s^3, a Higgs boson can be produced with large transverse momentum from gluon-gluon, quark-gluon, and quark-antiquark initial states. In the case of gluon-gluon collisions, the relevant Feynman diagrams are shown in Fig 4. The cross section for $g + g \rightarrow H + g$ can be written as,

$$\frac{d\sigma}{dt} = \frac{1}{16\pi s^2}\frac{1}{4V^2}\sum_{spins,colours}|M_3|^2 \ . \tag{2.1}$$

The invariant matrix element squared is given by,

$$\sum|M_3|^2 =$$
$$\alpha_W\alpha_S^3\frac{4NV}{stu}\frac{M_H^8}{M_W^2}\left[|A_2(s,t,u)|^2 + |A_2(u,s,t)|^2 + |A_2(t,u,s)|^2 + |A_4(s,t,u)|^2\right] . \tag{2.2}$$

The dimensionless functions A_2 and A_4 depend on the masses of the quarks in the internal loop. They are proportional to the gluon helicity amplitudes. Full analytic

results for A_2 and A_4 are given in the appendix.

The expression for $|M_3|^2$ simplifies considerably in the limit where the internal quark mass m_f becomes very large. In fact for a single flavour of very heavy quark we obtain,

$$\sum |M_3|^2 \to \alpha_W \alpha_S^3 \frac{4NV}{9} \left[\frac{M_H^8 + s^4 + t^4 + u^4}{stuM_W^2} \right]. \tag{2.3}$$

Note that, in the limit $m_f \to \infty$, a heavy quark gives a contribution independent of its mass. There is one factor of m_f from the Higgs quark-quark vertex and a second from the trace over the internal fermion loop. These are cancelled by a factor of $1/m_f^2$ from the integral over the internal loop momentum. The same effect occurs for the triangle graph shown in Fig. 1, which also produces a contribution independent of m_f at large values of m_f. Indeed in the limit $m_f \to \infty$, Eqs.(1.5) and (2.3) can both be obtained from an effective local interaction independent of m_f,

$$L_{eff} = \frac{\alpha_s}{24\pi} \frac{g_W}{M_W} F^A_{\alpha\beta} F_A^{\alpha\beta} H \ . \tag{2.4}$$

This heavy quark limit provides a consistency check on the exact calculation. The approximate form, Eq.(2.3), is much easier to use; we will discuss the accuracy of the approximation below.

Contributions from fermions with masses much less than M_H are suppressed by m_f^2/M_H^2. Hence only the top quark contribution is important for the range of Higgs masses relevant at the SSC. At the Tevatron collider where we will be interested in Higgs masses of order 10 GeV, the bottom quark will also be important and even the charm quark contribution cannot be ignored.

There is an additional contribution from the process $q + \overline{q} \to g + H$. In this case, the cross section is given by,

$$\frac{d\sigma}{dt} = \frac{1}{16\pi s^2} \frac{1}{4N^2} \sum |M_4|^2 \tag{2.5}$$

where the invariant matrix element is given by,

$$\sum_{spins,colours} |M_4|^2 = \alpha_W \alpha_S^3 V \frac{1}{2} \frac{(u^2 + t^2)}{sM_W^2} \frac{M_H^4}{(u+t)^2} |A_5|^2 \ . \tag{2.6}$$

The form factor A_5 is given in the appendix. Again the result simplifies in the limit

of large m_f.

$$\sum |M_4|^2 \rightarrow \alpha_W \alpha_S^3 V \frac{2}{9} \frac{u^2+t^2}{sM_W^2} \tag{2.7}$$

The final process is $q + g \rightarrow q + H$; the cross section is given by,

$$\frac{d\sigma}{dt} = \frac{1}{16\pi s^2} \frac{1}{4NV} \sum |M_5|^2 \ . \tag{2.8}$$

The matrix element can be obtained by crossing from that for $q + \overline{q} \rightarrow g + H$.

$$\sum |M_5(s,t,u)|^2 = -\sum |M_4(t,s,u)|^2 \tag{2.9}$$

III. Numerical Results

Fig. 5 shows the cross section $d\sigma/dp_t/dy$ as a function of the Higgs transverse momentum p_t in proton proton collisions at $\sqrt{s}$ of 40 TeV. The top quark mass has been set to 80 GeV. The structure functions of EHLQ[10] (set 2) have been used. We have chosen the scale Q^2 at which α_s and the structure functions are evaluated to be $m_H^2 + p_t^2$. Since the process is of third order in α_s, the rates are sensitive to this choice. If we use s, the square of the center of mass energy of the partonic system, the rates in Fig. 5 are reduced by a factor of 2 or so. It is also clear that the results are quite sensitive to the value of Λ; the set of structure functions used has $\Lambda = 0.29$ GeV. The sensitivity is much stronger at low values of m_H and p_t, where α_s and the structure functions are varying more rapidly with Q^2. We cannot know which scale is appropriate unless the order α_s^4 terms are calculated!

Fig. 5 also shows the rates predicted using the approximations to the matrix elements valid for large values of m_t. The accuracy of the approximation is determined by the kinematic region of interest. The approximation is good when m_t is larger than all of the kinematic invariants in the partonic scattering process. Clearly, for a top quark of mass 80 GeV and a Higgs mass of more than 100 GeV this can never be the case. Nevertheless the approximation is reasonably good at intermediate values of p_t. At large p_t the pointlike approximation seriously overestimates the rate. The approximation obviously improves at larger values of m_t. This can be seen from Fig. 6 which shows the production rates for a top quark mass of 160 GeV. Here again the approximation overestimates the rate at values of p_t where $p_t, M_H > m_t$.

Even at large p_t the total event rate is large. Fig. 7 shows the total cross section for Higgs bosons produced with transverse momentum greater than p_t^0. If we require transverse momenta of more than 100 GeV, so that we are in a region where the jet recoiling against the Higgs can be clearly seen, the cross section is of order 10 pb. By comparison with Fig. 2 we see that the requirement that the Higgs be produced in association with a large transverse momentum jet reduces the Higgs rate only by a factor of about ten.

The production rate of a light Higgs at the Tevatron collider is shown in Fig. 8. Notice the structure near $M_H = 2m_b$; this is due to the presence of the bottom quark in the triangle graph of Fig. 1. Fig. 9 shows the transverse momentum distribution at the Tevatron. In this figure we show the approximation with only one flavour (top) included. This is clearly the correct approximation at large values of p_t and M_H. However at smaller values the bottom quark can become important. This can clearly be seen from Fig. 9; the approximate rates fall considerably below the exact values at small p_t. If we were to include the bottom quark in the approximate rate, treating it as very heavy, then the approximate curves would increase by a factor of four providing a much better approximation at small p_t.

IV. Discussion and Conclusions

As we remarked in the introduction, the background for the Higgs signal we are looking at is the production of a tau pair at large transverse momentum via an intermediate virtual photon or Z. Fig. 10 shows the production of a pair of taus of invariant mass m as a function of transverse momentum of the pair at the SSC. In order to estimate the signal to background ratio we must multiply the rates from Figs. 5 or 6 by the branching ratio of the Higgs into a tau pair and must assume some value for the resolution in the tau pair invariant mass. If we take 10 GeV for the latter, then we obtain a signal and background curves shown in Fig. 11. As emphasized above, the exact value of the Higgs production rate and also the background is dependent upon the value of α_s. Fig. 11 shows that the signal is worst at values of M_H near to M_Z and at values near $2M_W$. The rapid fall off of the tau pair rate with the pair mass can be seen from Fig. 10; the tail of the Z is still visible at $m = 110$ GeV. It is this tail which compromises the signal to background at $M_H = 110$ GeV. At $M_H = 160$ GeV, the branching ratio into

tau pairs is becoming small owing to the decay to $Wf\bar{f}$. For intermediate values the signal to background ratio is reasonable. Since the tau pairs in the signal and background come from the decay of spin-0 and spin-1 particles respectively, the taus have different angular distributions relative to the direction of motion of their center of mass. This may be of use in extracting the signal.

There are two other possible sources of taus which could be important backgrounds. First, the production of a W pair in association with a jet, followed by the decay of both W's into $\tau\nu$. Since the total W pair production rate at the SSC is of order 0.1 nb,[10] this is unlikely to be a serious problem. Second is the production of a $b\bar{b}$ pair in association with a jet followed by the semileptonic decay of both b and $\bar{b}$ into taus. In this case there will be hadronic activity near the taus, from the hadrons produced in the semi-leptonic decay, which will be absent from the taus produced in Higgs decay. Given the large production rate for such $b\bar{b}$ pairs, this background deserves serious study involving Monte-Carlo simulations. Such a study is beyond the scope of this paper.

Taus themselves should be quite distinctive at the SSC. The leptonic decays are of course clean; but the hadronic modes should also be fairly easy to recognise since they produce jets with very low multiplicity and invariant mass. It is these two characteristics which have aided the UA1 collaboration[18] to reconstruct the decay $W \rightarrow \tau\nu$.

It is interesting to compare the signal in tau pairs with that from the decay of the Higgs into two photons. We will take the top quark mass to be 80 GeV since this will give the largest production rate (see Fig. 2). The background arises from the production of photons via quark-antiquark and gluon-gluon collisions.[19] The latter occurs via virtual quark loops; we have included it by using an approximation valid for quark masses much less than the photon pair invariant mass and have ignored the top quark. Its rate is about twice that from quark-antiquark annihilation; the large gluon distribution has overwhelmed the extra factor of α_s^2. Fig. 12 shows an estimate of the signal and background for photon pairs as a function of the Higgs mass. We have assumed a resolution of 3 GeV in the invariant mass of the photon pair and have forced the photons to be produced centrally in order to reduce the background. It can be seen that the signal to background ratio is much worse than in tau pair channel except for Higgs masses less than 110 GeV or greater than 155

GeV. There are also fewer events than in the tau pair mode. It is clear that both channels are difficult but promising and both are worthy of further study involving a detailed detector simulation. For this purpose the approximate forms of the Higgs production cross section at large p_t, Eqs.(2.3,2.7) are probably adequate.

Finally we would like to comment on the usefulness of the process in searching for a light Higgs at the Tevatron collider. The production rate is reasonable only for Higgs masses less than 20 GeV or so, as can be seen from Figs. 8 and 9. In order the estimate the background, we show in Fig. 13 the cross section for large p_t production of tau pairs via virtual photons and Z's at the Tevatron. A comparison of Figs. 9 and 13 shows that the signal to background ratio is worse than in the SSC case discussed above. The limiting factor at the Tevatron is more likely to be the small number of events, although if the Higgs is light enough for the decay into $b\bar{b}$ to be forbidden, the branching ratio into tau pairs is of order 25%. The situation may be improved in the case of Higgs bosons in non-standard models where the production rate may be enhanced.[20]

ACKNOWLEDGMENTS

We thank F. Paige for suggesting that Higgs production in association with a jet might lead to better mass resolution on the tau pair. We are grateful to M. Fontannaz, F. Halzen, Z. Kunszt and Z. Xu for discussions and to M. Veltman for use of the computer program FORMF, which yields the numerical values of one loop amplitudes and was used as a check of our analytic results. R.K.E. acknowledges the cordial hospitality of the University of Paris-Sud (Orsay) where part of this work was performed. I.H. would like to thank the Fermilab theory group for hospitality while this work was being done. The work of I.H. was supported by the Director, Office of Energy Research, Office of High Energy Physics, Division of High Energy Physics of the U.S. Department of Energy under Contract DE-AC03-76SF00098.

A APPENDIX - ANALYTIC FORMULAE.

The amplitude for gluon-gluon annihilation into a Higgs boson, or for the time reversed process $H \to g(p_1) + g(p_2)$ has been given in the literature[17]. In our

notation it may be written as,

$$M_{2\ AB}^{\ \alpha\beta} = \frac{-igwM_H^2}{M_W}\frac{g^2}{32\pi^2}\left(g^{\alpha\beta} - \frac{p_2^\alpha p_1^\beta}{p_1\cdot p_2}\right)\delta_{AB}\ A_1(M_H^2) \qquad (A.1)$$

where α(A) and β(B) are the Lorentz(colour) indices of gluons one and two. We have dropped terms which vanish because of the equations of motion for the gluon field. For a single flavour of quark of mass m_f the amplitude A_1 is given by,

$$A_1(M_H^2) = \frac{m_f^2}{M_H^2}\left[4 - W_2(M_H^2)(1 - \frac{4m_f^2}{M_H^2})\right] \qquad (A.2)$$

where W_2 is a transcendental function given below. After summing over colours and spins we obtain ($V = N^2 - 1 = 8$),

$$\sum |M_2|^2 = \frac{V}{8}\frac{\alpha_W\alpha_S^2}{\pi}\frac{M_H^4}{M_W^2}\left|A_1(M_H^2)\right|^2 . \qquad (A.3)$$

This matrix element squared is necessary for the calculation of Higgs production by two gluons and the width into two gluons. Eq. (A.3) simplifies in the limit $m_f \to \infty$ and becomes,

$$\sum |M_2|^2 = \frac{V}{18}\frac{\alpha_W\alpha_S^2}{\pi}\frac{M_H^4}{M_W^2}(1 + O(\frac{M_H^2}{m_f^2})) . \qquad (A.4)$$

The amplitude for the process,

$$H \to g(p_1) + g(p_2) + g(p_3) \qquad (A.5)$$

controls the decay of the Higgs into three gluons, and after crossing, the associated production of a Higgs particle and a gluon by two incoming gluons. Because of gauge invariance it can be expanded in terms of two invariant functions A_2 and A_3.

$$M_{3\ ABC}^{\ \alpha\beta\gamma} = \frac{g_W M_H^4}{M_W}\frac{g^3}{32\pi^2}\left\{f_{ABC}\frac{p_1^\gamma}{p_1\cdot p_3}\left[\left(\frac{p_2^\alpha p_1^\beta}{(p_1\cdot p_2)^2} - \frac{g^{\alpha\beta}}{p_1\cdot p_2}\right)A_2(s,t,u) + \frac{g^{\alpha\beta}}{p_1\cdot p_2}A_3(s,t,u)\right]\right.$$
$$\left. + \frac{1}{3}f_{ABC}\frac{p_3^\alpha p_1^\beta p_2^\gamma A_3(s,t,u)}{p_1\cdot p_2\ p_2\cdot p_3\ p_3\cdot p_1}\right\} + \left\{\text{permutations}\right\} \qquad (A.6)$$

f_{ABC} is the structure constant of $SU(N)$. We have dropped terms which vanish by the equation of motion for the gluon field. The permutations not written explicitly

in Eq.(A.6) are the five exchanges of p_1, p_2, and p_3 (and their associated colour and Lorentz indices) necessary to impose full Bose symmetry. In calculating the amplitude for the process Eq.(A.5) we define $s = (p_1 + p_2)^2, t = (p_1 + p_3)^2, u = (p_2 + p_3)^2$ so that after crossing to the production process we obtain the normal definitions of t and u. The function A_2 is symmetric under the exchange of its last two arguments whereas A_3 is a totally symmetric function of its arguments. The invariant cross section is most easily defined in terms of the helicity amplitudes A_2 and A_4, where A_4 is given by,

$$A_4(s,t,u) = [A_2(s,t,u) + A_2(u,s,t) + A_2(t,u,s) - 2A_3(s,t,u)] \ . \qquad (A.7)$$

The invariant cross section in terms of these amplitudes is given in Eqs. (2.1) and (2.2). Because of the properties of A_3 and A_2, the function A_4 is also totally symmetric under the interchange of its arguments, and hence can be written,

$$A_4(s,t,u) = [b_4(s,t,u) + b_4(u,s,t) + b_4(t,u,s)] \ . \qquad (A.8)$$

In a similar way, A_2 which is symmetric in its last two arguments, may be written

$$A_2(s,t,u) = [b_2(s,t,u) + b_2(s,u,t)] \ . \qquad (A.9)$$

To the order in perturbation theory to which we are working, the auxiliary functions b_4, b_2 are given by † (for a single flavour of quark of mass m_f),

$$b_4(s,t,u) = \frac{m_f^2}{M_H^2}\left[-\frac{2}{3} + \left(\frac{m_f^2}{M_H^2} - \frac{1}{4}\right)\left(W_2(s) - W_2(M_H^2) + W_3(s,t,u,M_H^2)\right)\right] \qquad (A.10)$$

$$\begin{aligned} b_2(s,t,u) = \frac{m_f^2}{M_H^4}\Bigg[& \frac{s(u-s)}{s+u} + \frac{2ut(u+2s)}{(s+u)^2}\left(W_1(t) - W_1(M_H^2)\right) \\ & + (m_f^2 - \frac{s}{4})\left(\frac{1}{2}W_2(s) + \frac{1}{2}W_2(M_H^2) - W_2(t) + W_3(s,t,u,M_H^2)\right) \\ & + s^2\left(\frac{2m_f^2}{(s+u)^2} - \frac{1}{2(s+u)}\right)(W_2(t) - W_2(M_H^2)) + \frac{ut}{2s}(W_2(M_H^2) - 2W_2(t)) \\ & + \frac{1}{8}\left(s - 12m_f^2 - \frac{4ut}{s}\right)W_3(t,s,u,M_H^2)\Bigg] \ . \end{aligned} \qquad (A.11)$$

† We have found the techniques of Ref. 21 to be invaluable in performing the calculation.

W_1, W_2 and W_3 are auxiliary functions given below. In the limit $m_f \to \infty$, the values of A_2 and A_4 are,

$$A_4(s,t,u) \to -\frac{1}{3}, \quad A_2(s,t,u) \to -\frac{s^2}{3M_H^4} \ . \tag{A.12}$$

Lastly we consider the process $q(p_1) + \bar{q}(p_2) \to H + g(p_3)$. The invariant amplitude is given by,

$$M_4^{\gamma}{}_C = \frac{ig_W M_H^2}{sM_W} \frac{g^3}{32\pi^2} \overline{v}(-p_2)\gamma^{\alpha} t_C u(p_1) \left(g^{\alpha\gamma} - \frac{p_3^{\alpha}(p_1^{\gamma} + p_2^{\gamma})}{(p_1+p_2)\cdot p_3} \right) A_5 \tag{A.13}$$

where with a single flavour of quark in the internal loop we obtain,

$$A_5 = \frac{m_f^2}{M_H^2} \left[4 + \frac{4s}{u+t} \Big(W_1(s) - W_1(M_H^2) \Big) + \Big(1 - \frac{4m_f^2}{u+t} \Big) \Big(W_2(s) - W_2(M_H^2) \Big) \right] \ . \tag{A.14}$$

The transcendental functions W_1, W_2 and W_3 are defined by,

$$W_1(s) = 2 + \int_0^1 dx \ln\left(1 - \frac{s}{m_f^2} x(1-x) - i\epsilon\right) \tag{A.15}$$

$$W_2(s) = 2\int_0^1 \frac{dx}{x} \ln\left(1 - \frac{s}{m_f^2} x(1-x) - i\epsilon\right) \tag{A.16}$$

$$W_3(s,t,u,v) = I_3(s,t,u,v) - I_3(s,t,u,s) - I_3(s,t,u,u) \tag{A.17}$$

$$I_3(s,t,u,v) = \int_0^1 dx \left(\frac{m_f^2 t}{us} + x(1-x)\right)^{-1} \ln\left(1 - \frac{v}{m_f^2} x(1-x) - i\epsilon\right) \ . \tag{A.18}$$

They have the following values (see also ref.(22)),

$$\begin{aligned} W_1(s) &= 2(1 - \tfrac{4m_f^2}{s})^{1/2} \operatorname{arcsinh}(\tfrac{\sqrt{-s}}{2m_f}), && s < 0 \\ &= 2(\tfrac{4m_f^2}{s} - 1)^{1/2} \arcsin(\tfrac{\sqrt{s}}{2m_f}), && 0 < s < 4m_f^2 \\ &= (1 - \tfrac{4m_f^2}{s})^{1/2} (2 \operatorname{arccosh}(\tfrac{\sqrt{s}}{2m_f}) - i\pi), && s > 4m_f^2 \end{aligned} \tag{A.19}$$

$$\begin{aligned} W_2(s) &= 4(\operatorname{arcsinh}(\tfrac{\sqrt{-s}}{2m_f}))^2, && s < 0 \\ &= -4(\arcsin(\tfrac{\sqrt{s}}{2m_f}))^2, && 0 < s < 4m_f^2 \\ &= 4(\operatorname{arccosh}(\tfrac{\sqrt{s}}{2m_f}))^2 - \pi^2 - 4i\pi \operatorname{arccosh}(\tfrac{\sqrt{s}}{2m_f}), && s > 4m_f^2 \ . \end{aligned} \tag{A.20}$$

$$
\begin{aligned}
I_3(s,t,u,v) &= \tfrac{2}{2\beta-1}[-\mathrm{Li}_2(\tfrac{\gamma}{\gamma+\beta-1})+\mathrm{Li}_2(\tfrac{\gamma-1}{\gamma+\beta-1}) \\
&\quad +\mathrm{Li}_2(\tfrac{\beta-\gamma}{\beta})-\mathrm{Li}_2(\tfrac{\beta-\gamma}{\beta-1}) \\
&\quad +(\log^2\beta-\log^2(\beta-1))/2 \\
&\quad +\log\gamma\,\log(\tfrac{\gamma+\beta-1}{\beta}) \\
&\quad +\log(\gamma-1)\,\log(\tfrac{\beta-1}{\gamma+\beta-1})], \qquad v<0 \\
&= \tfrac{2}{2\beta-1}[2\mathrm{Li}_2(r,\theta)-2\mathrm{Li}_2(r,\phi) \\
&\quad +(\phi-\theta)(\phi+\theta-\pi)], \qquad 0<v<4m_f^2 \\
&= \tfrac{2}{2\beta-1}[-\mathrm{Li}_2(\tfrac{\gamma}{\gamma+\beta-1})+\mathrm{Li}_2(\tfrac{\gamma-1}{\gamma+\beta-1}) \\
&\quad +\mathrm{Li}_2(\tfrac{\gamma}{\gamma-\beta})-\mathrm{Li}_2(\tfrac{\gamma-1}{\gamma-\beta}) \\
&\quad +\log(\tfrac{\gamma}{1-\gamma})\,\log(\tfrac{\gamma+\beta-1}{\beta-\gamma}) \\
&\quad -i\pi\log(\tfrac{\gamma+\beta-1}{\beta-\gamma})], \qquad v>4m_f^2
\end{aligned}
\tag{A.21}
$$

with,

$$
\begin{aligned}
\beta &= \tfrac{1}{2}(1+\sqrt{1+\tfrac{4tm_f^2}{us}}), \\
\gamma &= \tfrac{1}{2}(1+\sqrt{1-\tfrac{4m_f^2}{v}}), \\
a &= \sqrt{\tfrac{4m_f^2}{v}-1}, \\
r^2 &= \tfrac{a^2+1}{a^2+(2\beta-1)^2}, \\
\cos\phi &= \tfrac{r(a^2+2\beta-1)}{1+a^2}, \\
\cos\theta &= \tfrac{r(a^2-2\beta+1)}{1+a^2}, \qquad 0<\theta,\phi<\pi.
\end{aligned}
\tag{A.22}
$$

Finally the dilogarithms are defined by,

$$\mathrm{Li}_2(x) = -\int_0^x \frac{\log(1-z)}{z}dz$$

and

$$\mathrm{Li}_2(x,\theta) = -\frac{1}{2}\int_0^x \frac{\log(1-2z\cos\theta+z^2)}{z}dz\ .$$

REFERENCES

1. S. Glashow, *Nucl. Phys.* 22:579 (1961);
S. Weinberg, *Phys. Rev. Lett.* 19:1264 (1967);
A. Salam, *in*: "Elementary Particle Theory," W. Svartholm, ed., Almquist and Wiksell, Stockholm (1968).

2. S. Weinberg *Phys. Rev. Lett.* 36:294 (1976);
A. Linde, *JETP Lett.* 23:64 (1976);
E. Witten, *Nucl. Phys. B177*: 477 (1981);
A. Guth and E. Weinberg, *Phys. Rev. Lett.* 65:1131 (1980).

3. B.W. Lee, C. Quigg and H. Thacker, *Phys. Rev. D* 16:1519 (1977);
M. Veltman, *Acta Phys. Polon.* B8:475 (1977).

4. E. Farhi and L. Susskind, *Phys. Rep.* 74:277 (1981);
M. Chanowitz and M.K. Gaillard, *Nucl. Phys.*, B261:379 (1985).

5. For a recent review see, for example, J. Ellis in "New Frontiers in Particle Physics", ed. J.M. Cameron, B.A. Campbell, A.N. Kamal and F.C. Khanna, World Scientific Publishing Company, Singapore, 1987.

6. J.D. Bjorken, *in*: "Proceedings of the 1976 SLAC Summer Institute," M. Zipf, ed.

7. B.L. Ioffe and V.A. Khoze, Leningrad report LINP-274 (1976).

8. F. Wilczek, *Phys. Rev. Lett.* 39:1304 (1977);
M. I. Vysotsky, *Phys. Lett. 97B*: 159 (1980).

9. H. Gordon *et al.*, *Proc. 1982 Summer Study on the Design and Utilization of the Superconducting Super Collider*, R. Donaldson, R Gustafson and F. Paige, (eds.), Fermilab, Batavia, Illinois, 1984, p. 161
R. Cahn and M. Chanowitz, *Phys. Rev.Lett.* 56:1327 (1986).

10. E. Eichten et al., *Rev. Mod. Phys.* 56:579 (1986).

11. J.F. Gunion *et al., Phys. Rev.Lett.* 54:1226 (1985); *Phys. Rev. D* 34:101 (1986).

12. F.J. Gilman and B. Cox *Proc. 1984 Summer Study on the Design and Utilization of the Superconducting Super Collider*, R. Donaldson and J. Morfin (eds.), Fermilab, Batavia, Illinois, 1985.

13. H. Albrecht *et al.*, DESY-87-029 (1987);
F.J. Gilman, SLAC-PUB-4315 (1987).

14. W.-Y. Keung and W. Marciano *Phys. Rev.*D30:248 (1984).

15. F.J. Gilman and L. Price, *Proc. 1986 Summer Study on the Design and Utilization of the Superconducting Super Collider*, R. Donaldson and J. Marx (eds.), Fermilab, Batavia, Illinois, 1987.

16. A. Vainshtein *et al.*, *Sov. Phys.-Usp.23*: 429 (1980).

17. H. Georgi *et al.*, *Phys. Rev. Lett. 40*: 692 (1978).

18. C. Albajar *et al. Phys. Lett. 185B*: 233 (1987).

19. B. Combridge, *Nucl. Phys. B174*: 243 (1980).

20. E. Eichten *et al., Phys. Rev.*, D34:1547 (1986).

21. G. Passarino and M. Veltman, *Nucl. Phys. B160*: 151 (1979).

22. B. De Tollis, *Nuovo Cim.[10]32*: 757 (1964).

FIGURE CAPTIONS

Figure 1: Feynman diagram showing the process $H \rightarrow gluon+gluon$. Also shown are the momenta of the gluons as well as their spin and colour indices.

Figure 2: The cross section $d\sigma/dy$ at $y = 0$ for the production of a Higgs boson at $\sqrt{s} = 40$ TeV, as a function of the Higgs mass. The solid, dashed and dot-dashed lines correspond to top quark masses of 80 GeV, 120 GeV and 160 GeV respectively.

Figure 3: The cross section $d\sigma/dm/dy$ at $y = 0$ for the production of a tau pair at $\sqrt{s} = 40$ TeV, as a function of the pair mass (m).

Figure 4: Feynman diagram showing the process $H \rightarrow gluon + gluon + gluon$. Also shown are the momenta of the gluons as well as their spin and colour indices. The amplitude for the production process can be obtained by crossing.

Figure 5: The cross section $d\sigma/dp_t/dy$ for the production of a Higgs boson at rapidity $y = 0$ as a function of the transverse momentum p_t of the Higgs boson at $\sqrt{s} = 40$ TeV. The top quark mass has been set to 80 GeV for the exact calculation. Results for the exact and approximate matrix elements are shown.

Figure 6: As for Fig. 5 except that the top quark mass has been set to 160 GeV. Notice that the approximate curves (dotted and dot-dashed lines) are identical to those in Fig. 5, since the approximate matrix element is independent of m_t.

Figure 7: The cross section for the production of a Higgs boson in proton proton collisions at $\sqrt{s} = 40$ TeV with transverse momentum greater than p_t^0 as a function of p_t^0. The top quark mass has been set to 80 GeV.

Figure 8: The cross section $d\sigma/dy$ at $y = 0$ for the production of a Higgs boson in proton antiproton collisions at $\sqrt{s} = 1.8\ TeV$, as a function of the Higgs mass. The solid and dashed lines correspond to top quark masses of 30 GeV and 80 GeV respectively.

Figure 9: The cross section $d\sigma/dp_t/dy$ for the production of a Higgs boson at rapidity $y = 0$ as a function of the transverse momentum p_t of the Higgs boson in proton antiproton collisions at $\sqrt{s} = 1.8$ TeV. The top quark mass has been set to 30 GeV. Only one flavour (the top) is included in the approximate form (see text).

Figure 10: The cross section $d\sigma/dp_t/dm/dy$ for the production of a lepton pair in proton proton collisions at $\sqrt{s} = 40$ TeV via intermediate virtual photons and Z's at rapidity $y = 0$ as a function of the transverse momentum p_t of the lepton pair. The solid, dotted, dashed and dot-dashed curves correspond to pair masses of 110, 125, 140 and 160 GeV respectively.

Figure 11: Signal and background curves at $y = 0$ as a function of p_t for the production of higgs boson followed by its decay to a tau pair. The signal (solid lines) is obtained by multiplying the rates of Fig. 5 by the appropriate branching ratio. The background (dashed lines) is obtained

from the continuum tau pair rate viz. $d\sigma/dm/dp_t/dy \times \Delta m$, evaluated at $m = M_H$. The resolution Δm has been taken to be 10 GeV.

Figure 12: An estimate of the signal and background in the channel $H \to \gamma\gamma$. Both photons are required to have rapidity $|y| < 1.5$. The signal (solid line) is obtained by multiplying the production rate from the mechanism of Fig. 1 by the branching ratio into $\gamma\gamma$. The background (dashed line) is estimated from $d\sigma/dm \times \Delta m$ for the production of a pair of photons of invariant mass $m = M_H$. A resolution of 3 GeV in the photon pair mass (Δm) has been assumed.

Figure 13: The cross section $d\sigma/dp_t/dm/dy$ for the production of a lepton pair in proton antiproton collisions at $\sqrt{s} = 1.8\ TeV$ via intermediate virtual photons and Z's at rapidity $y = 0$ as a function of the transverse momentum p_t of the pair. The curves (top to bottom) correspond to pair masses of 7, 14 and 21 GeV.

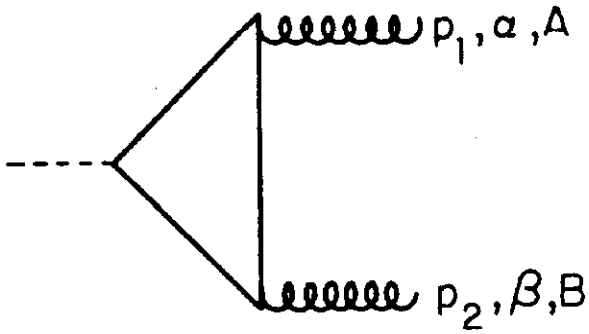

Figure 1

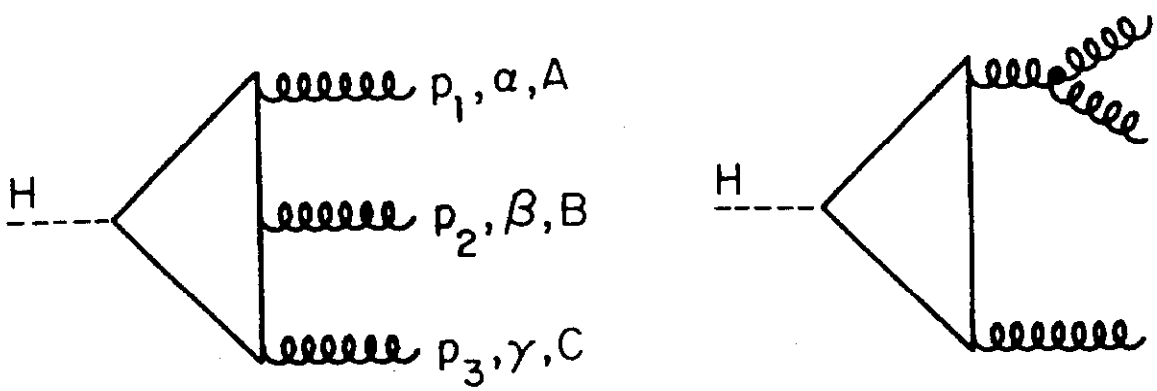

Figure 4

Figure 2

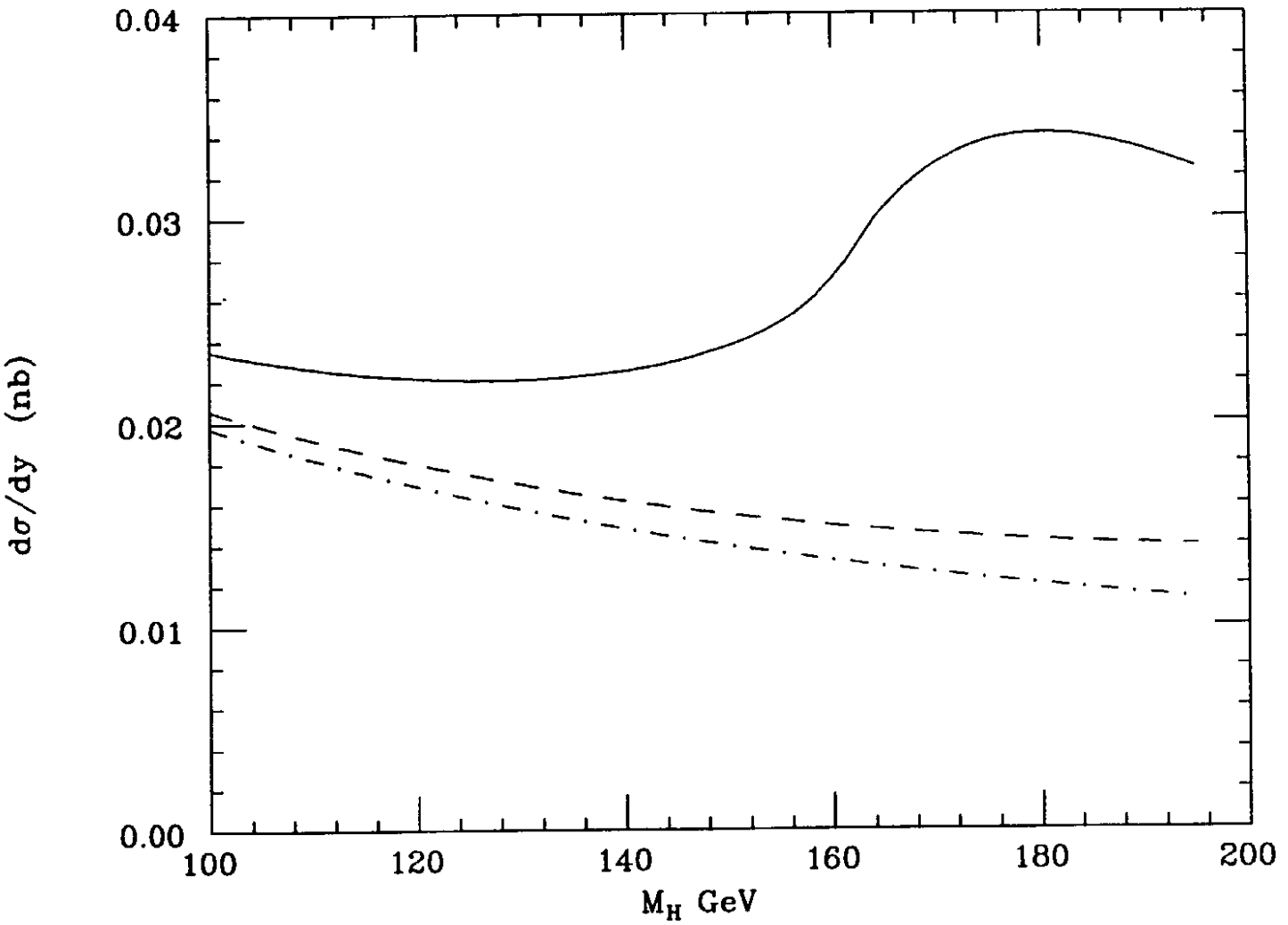

Figure 3

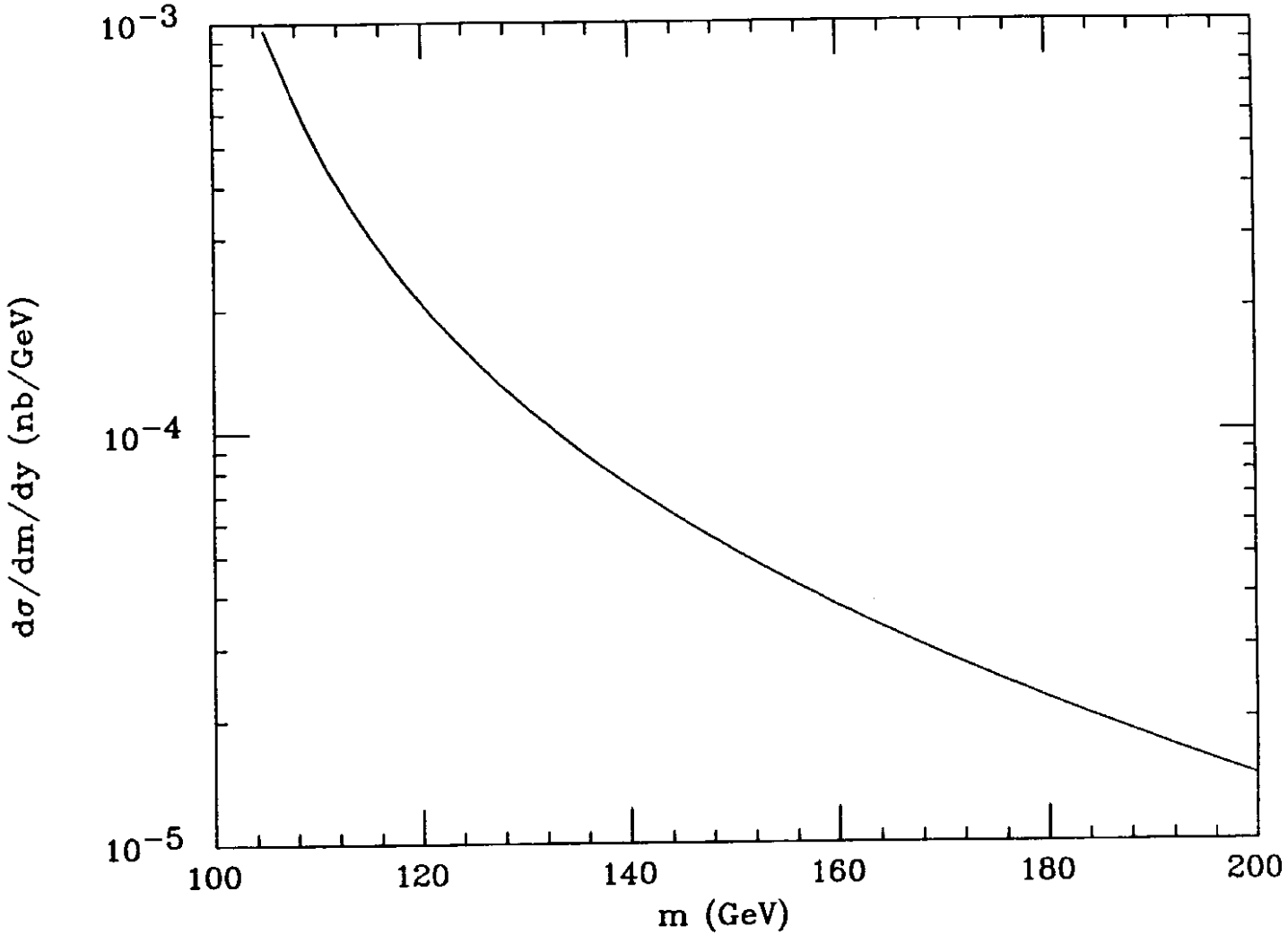

Figure 5

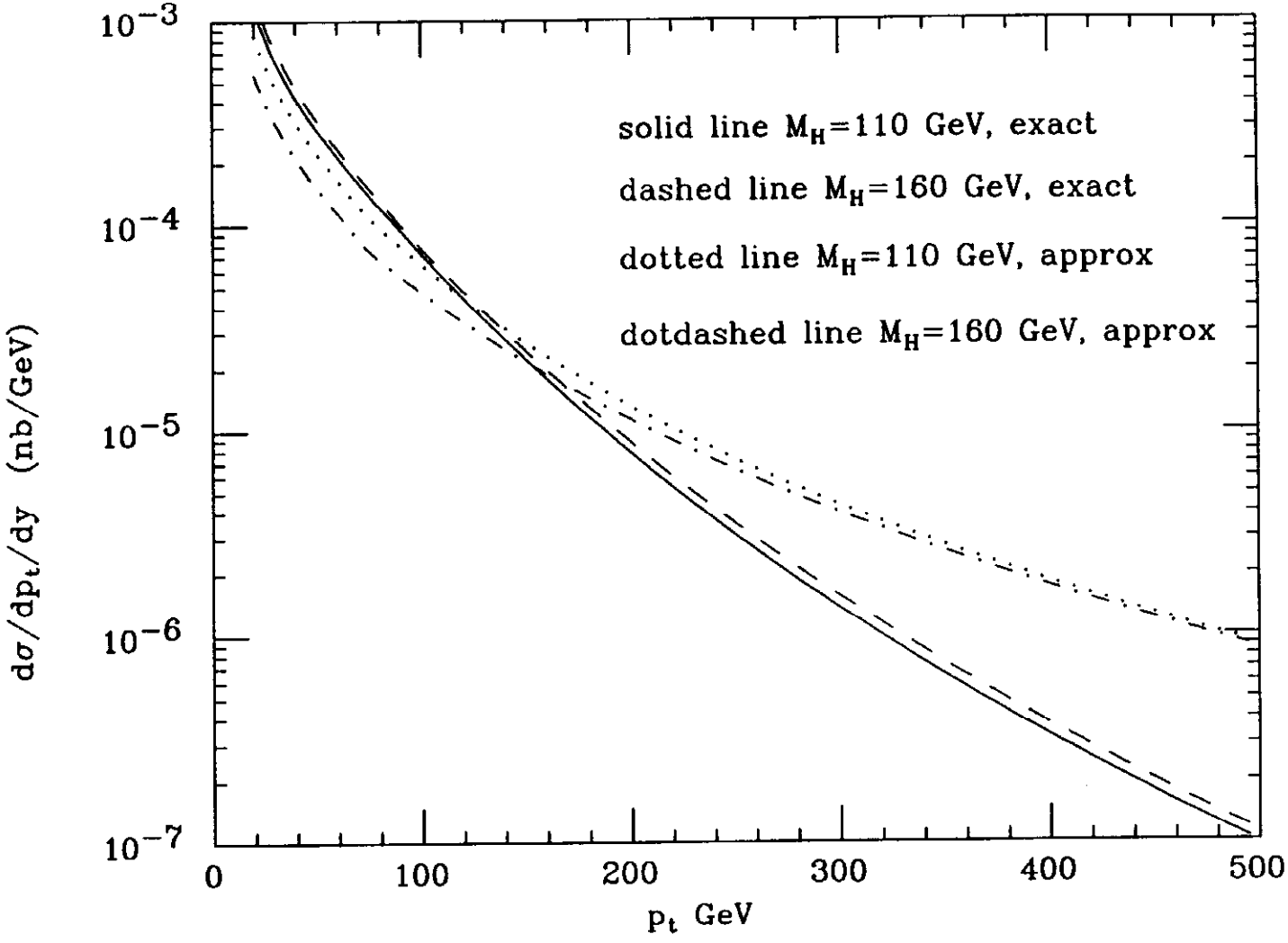
10^{-3}
10^{-4}
10^{-5}
10^{-6}
10^{-7}
$d\sigma/dp_t/dy$ (nb/GeV)
0
100
200
300
400
500
p_t GeV
solid line M_H=110 GeV, exact
dashed line M_H=160 GeV, exact
dotted line M_H=110 GeV, approx
dotdashed line M_H=160 GeV, approx

Figure 6

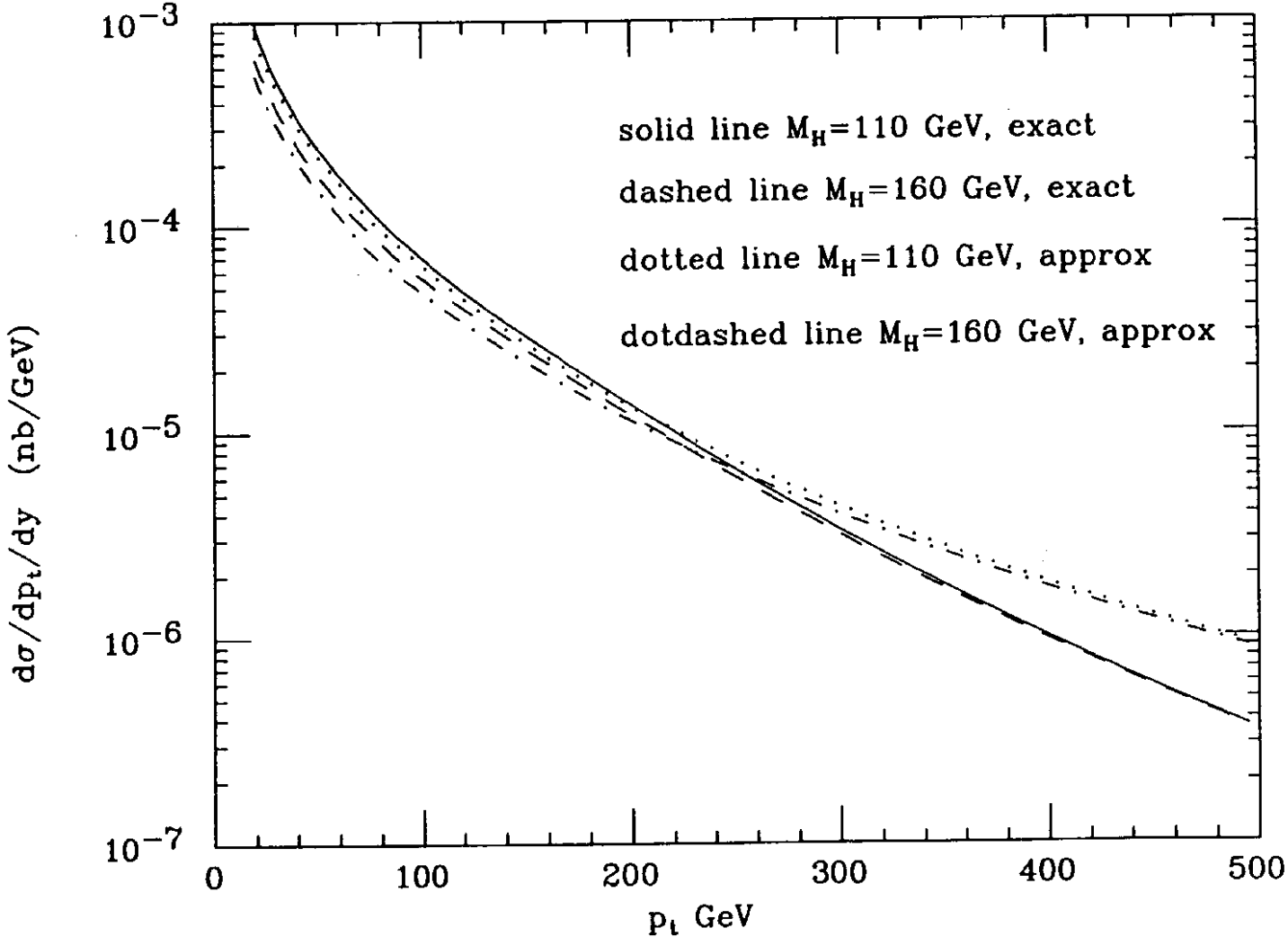
solid line M_H=110 GeV, exact
dashed line M_H=160 GeV, exact
dotted line M_H=110 GeV, approx
dotdashed line M_H=160 GeV, approx
$d\sigma/dp_t/dy$ (nb/GeV)
10^{-3}
10^{-4}
10^{-5}
10^{-6}
10^{-7}
0
100
200
300
400
500
p_t GeV

Figure 7

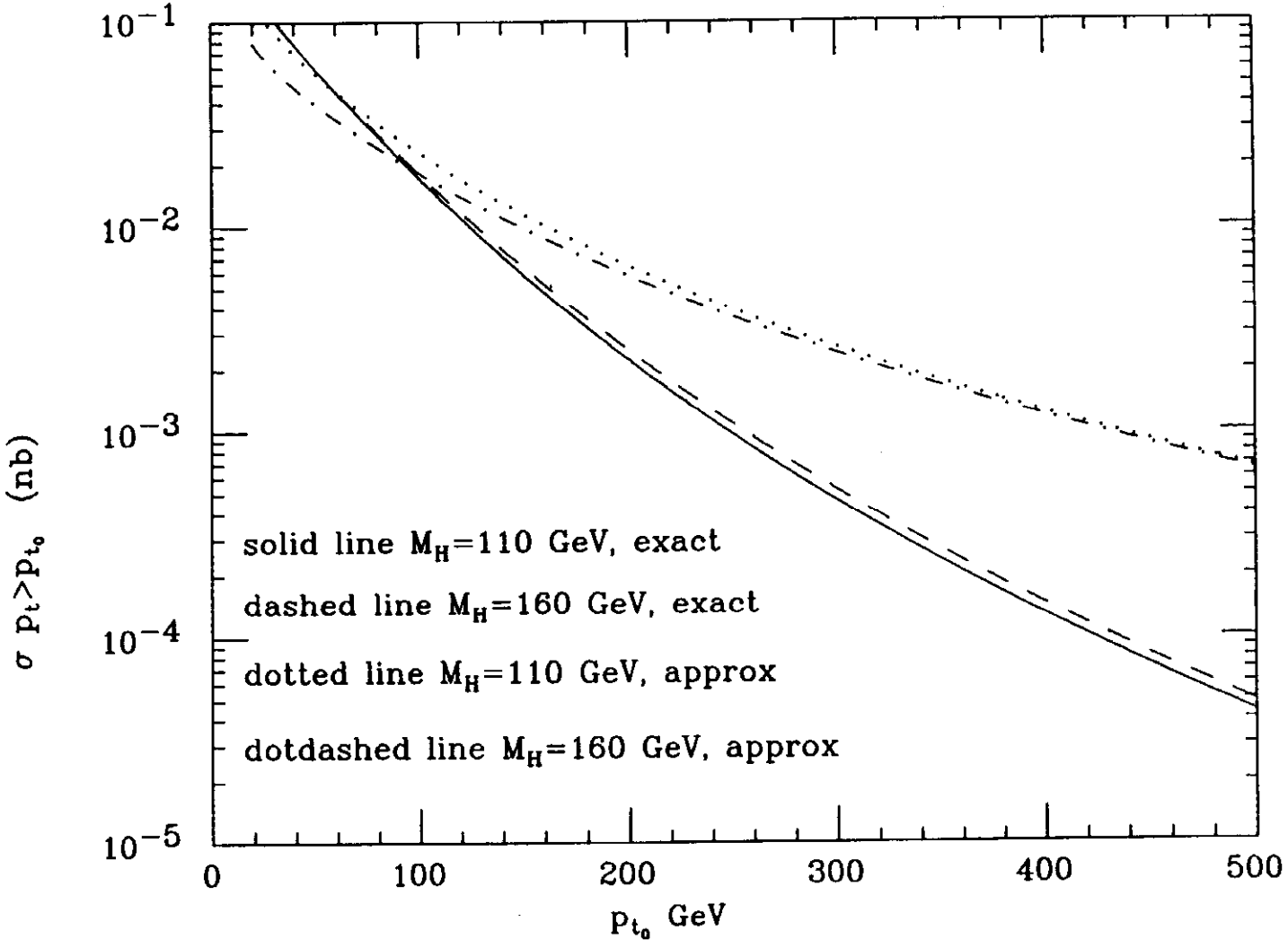
10^{-1}
10^{-2}
10^{-3}
10^{-4}
10^{-5}
$\sigma\ p_t > p_{t_0}$ (nb)
solid line M_H=110 GeV, exact
dashed line M_H=160 GeV, exact
dotted line M_H=110 GeV, approx
dotdashed line M_H=160 GeV, approx
0
100
200
300
400
500
p_{t_0} GeV

Figure 8

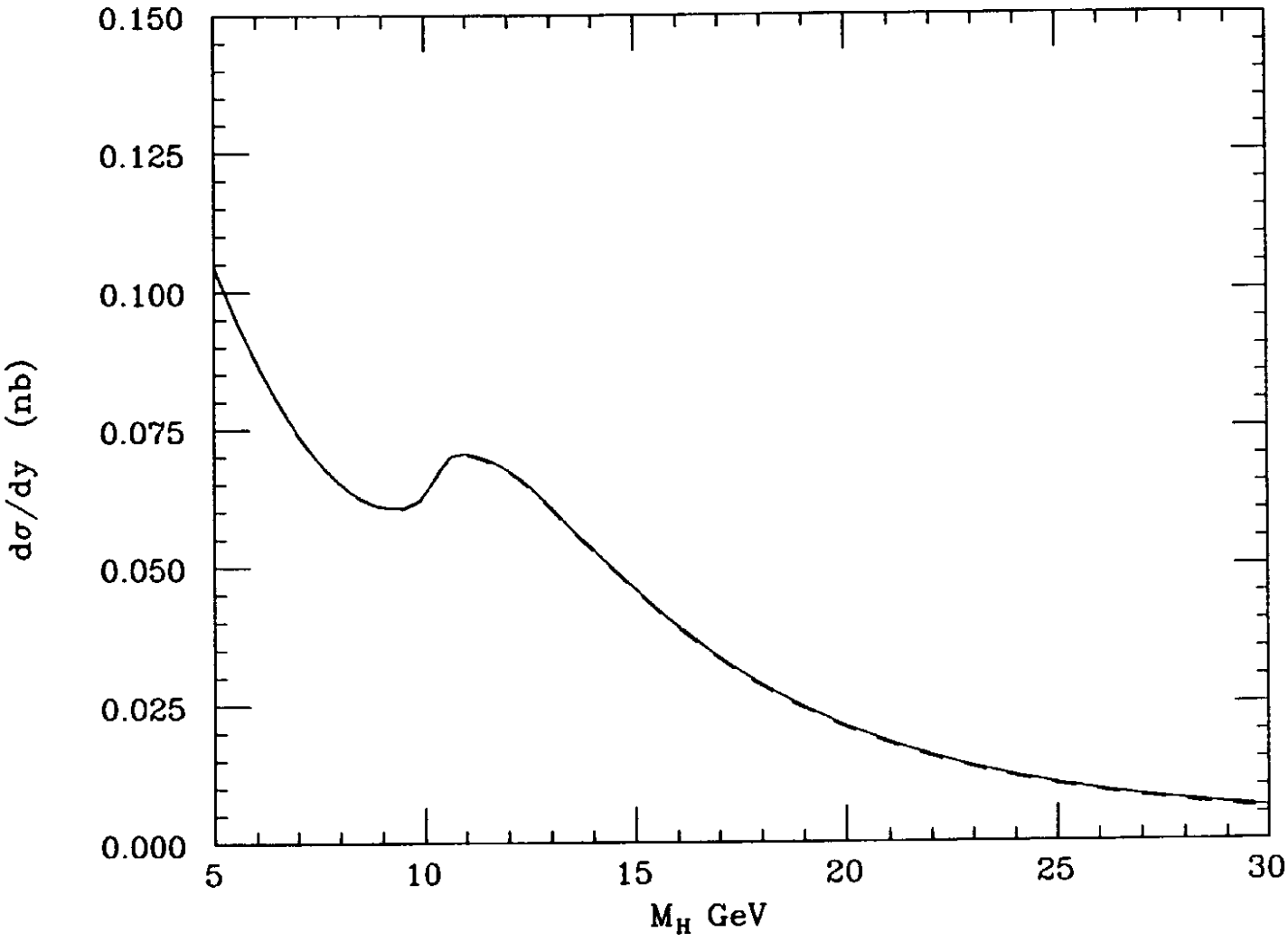
0.150
0.125
0.100
0.075
0.050
0.025
0.000
dσ/dy (nb)
5
10
15
20
25
30
M_H GeV

Figure 9

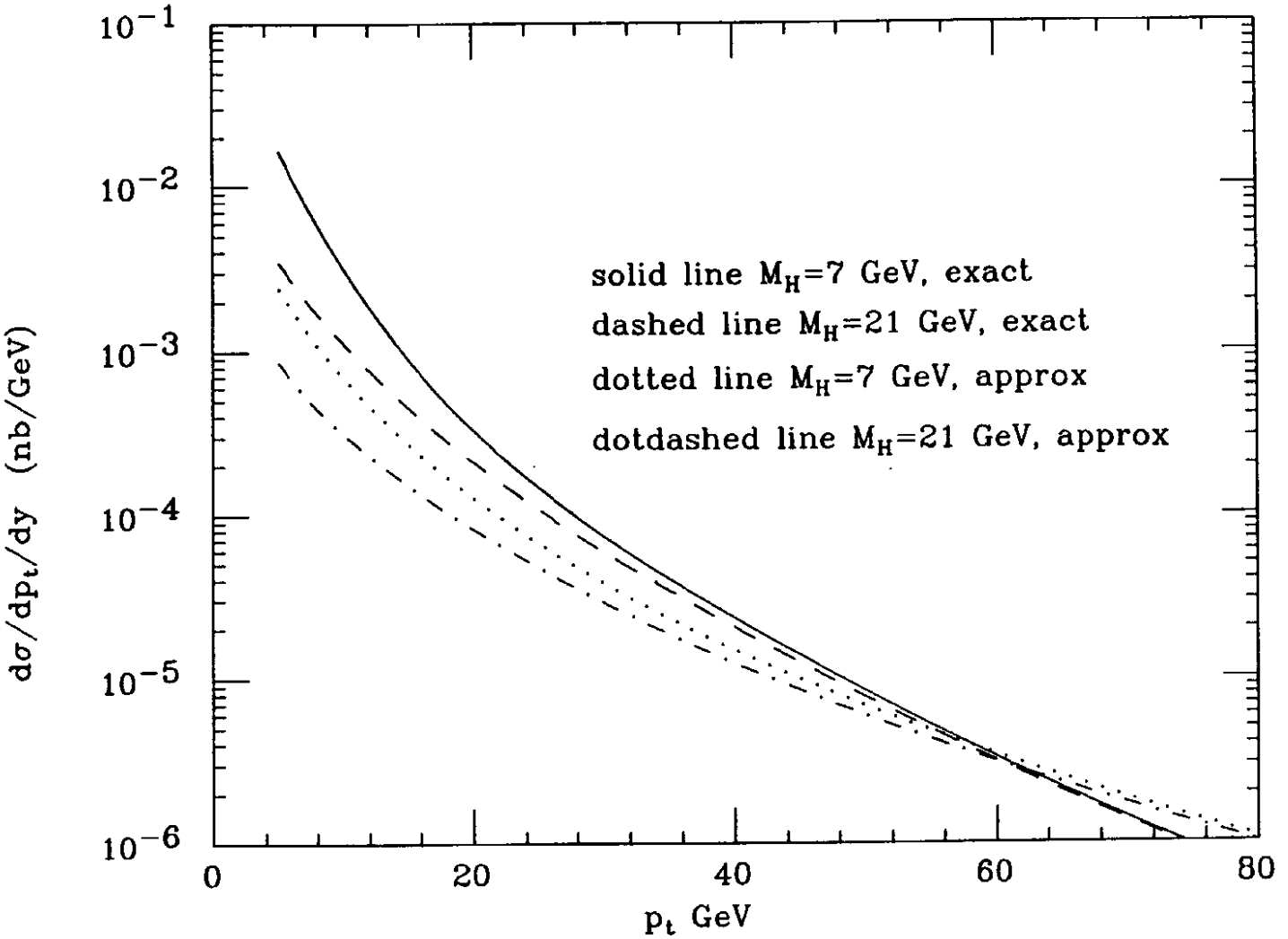
10^{-1}
10^{-2}
10^{-3}
10^{-4}
10^{-5}
10^{-6}
$d\sigma/dp_t/dy$ (nb/GeV)
0
20
40
60
80
p_t GeV
solid line M_H=7 GeV, exact
dashed line M_H=21 GeV, exact
dotted line M_H=7 GeV, approx
dotdashed line M_H=21 GeV, approx

Figure 10

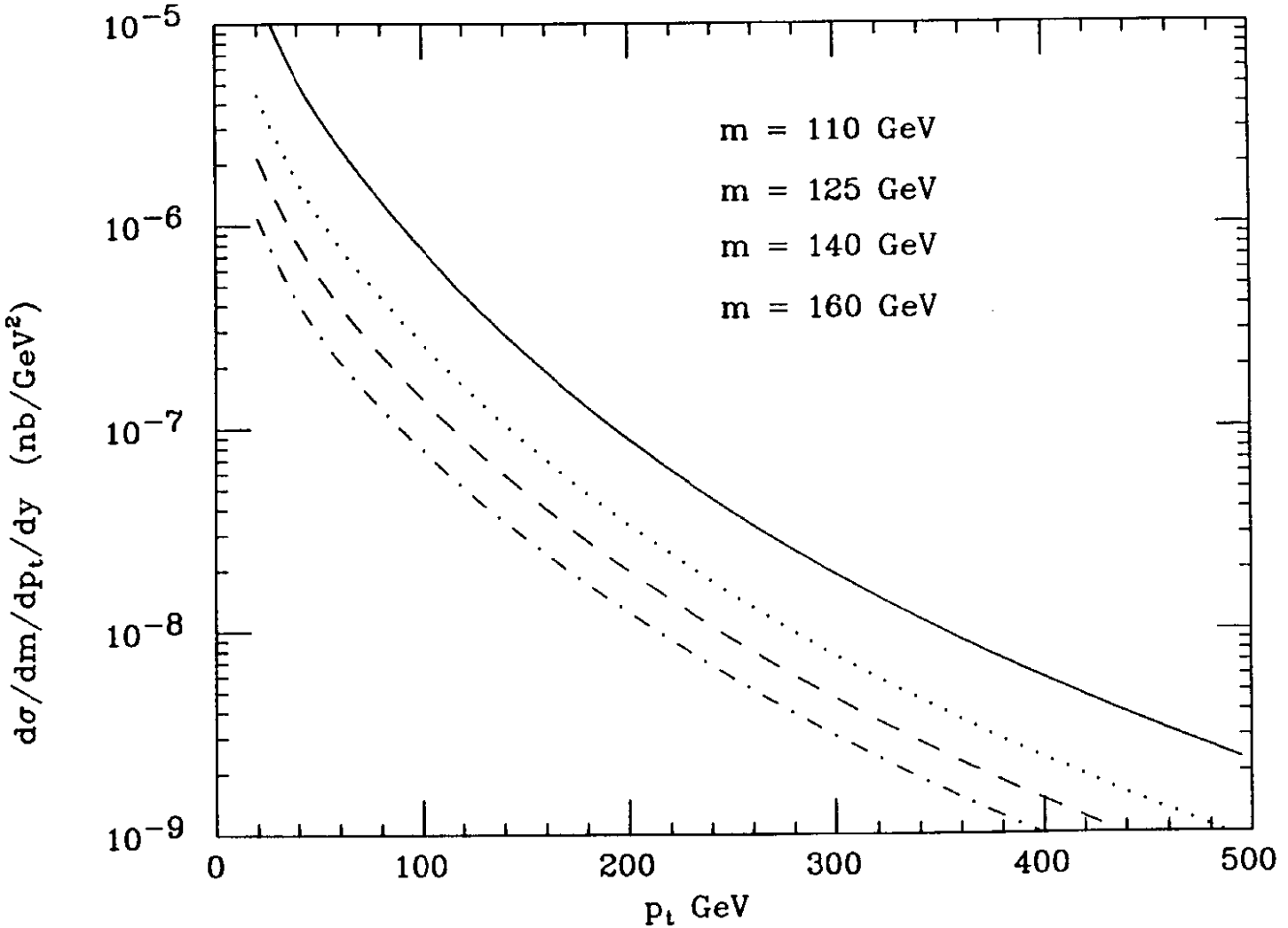
10^{-5}
10^{-6}
10^{-7}
10^{-8}
10^{-9}
$d\sigma/dm/dp_t/dy$ (nb/GeV^2)
m = 110 GeV
m = 125 GeV
m = 140 GeV
m = 160 GeV
0
100
200
300
400
500
p_t GeV

Figure 11

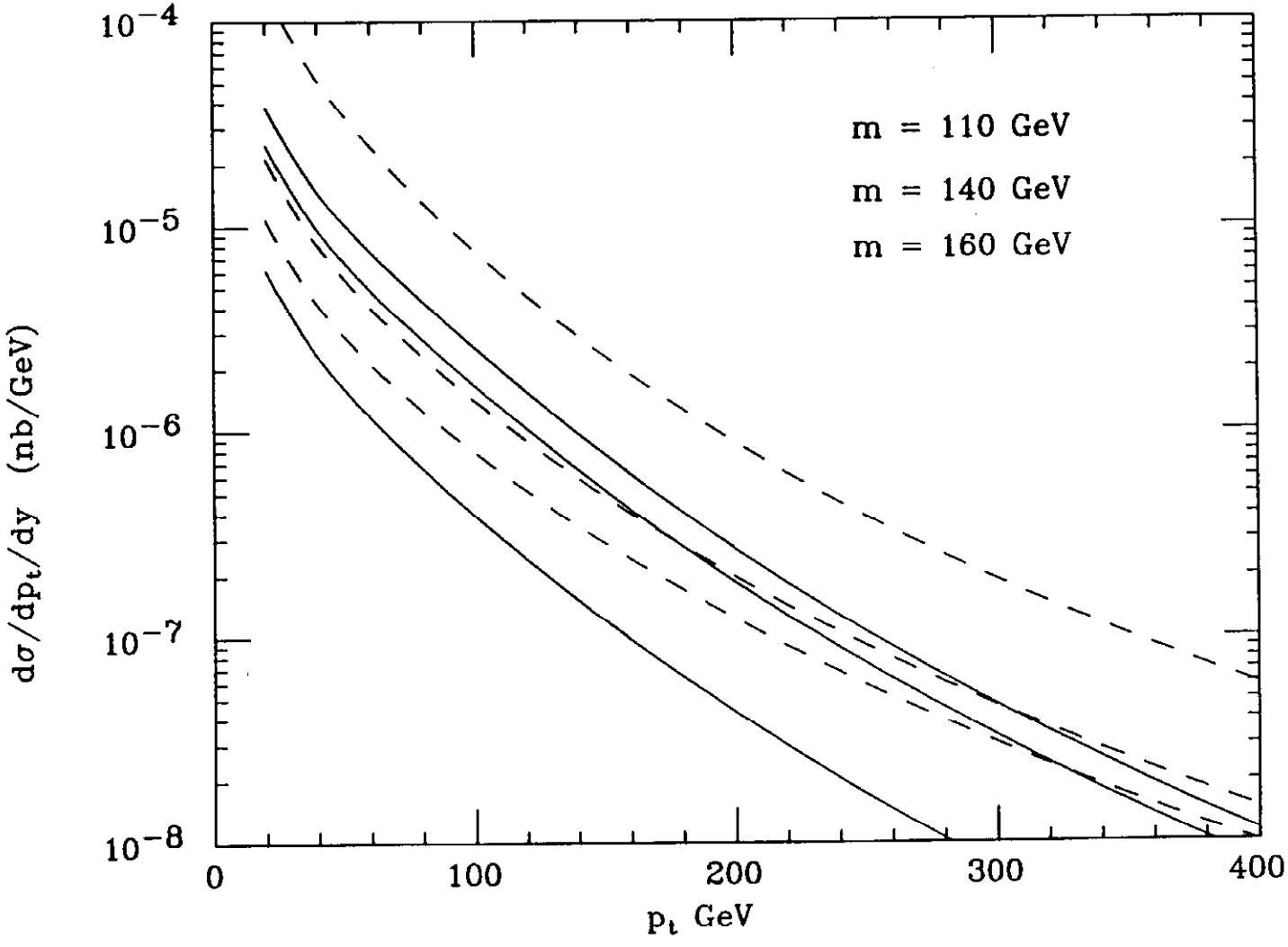
10^{-4}
10^{-5}
10^{-6}
10^{-7}
10^{-8}
$d\sigma/dp_t/dy$ (nb/GeV)
m = 110 GeV
m = 140 GeV
m = 160 GeV
0
100
200
300
400
p_t GeV

Figure 12

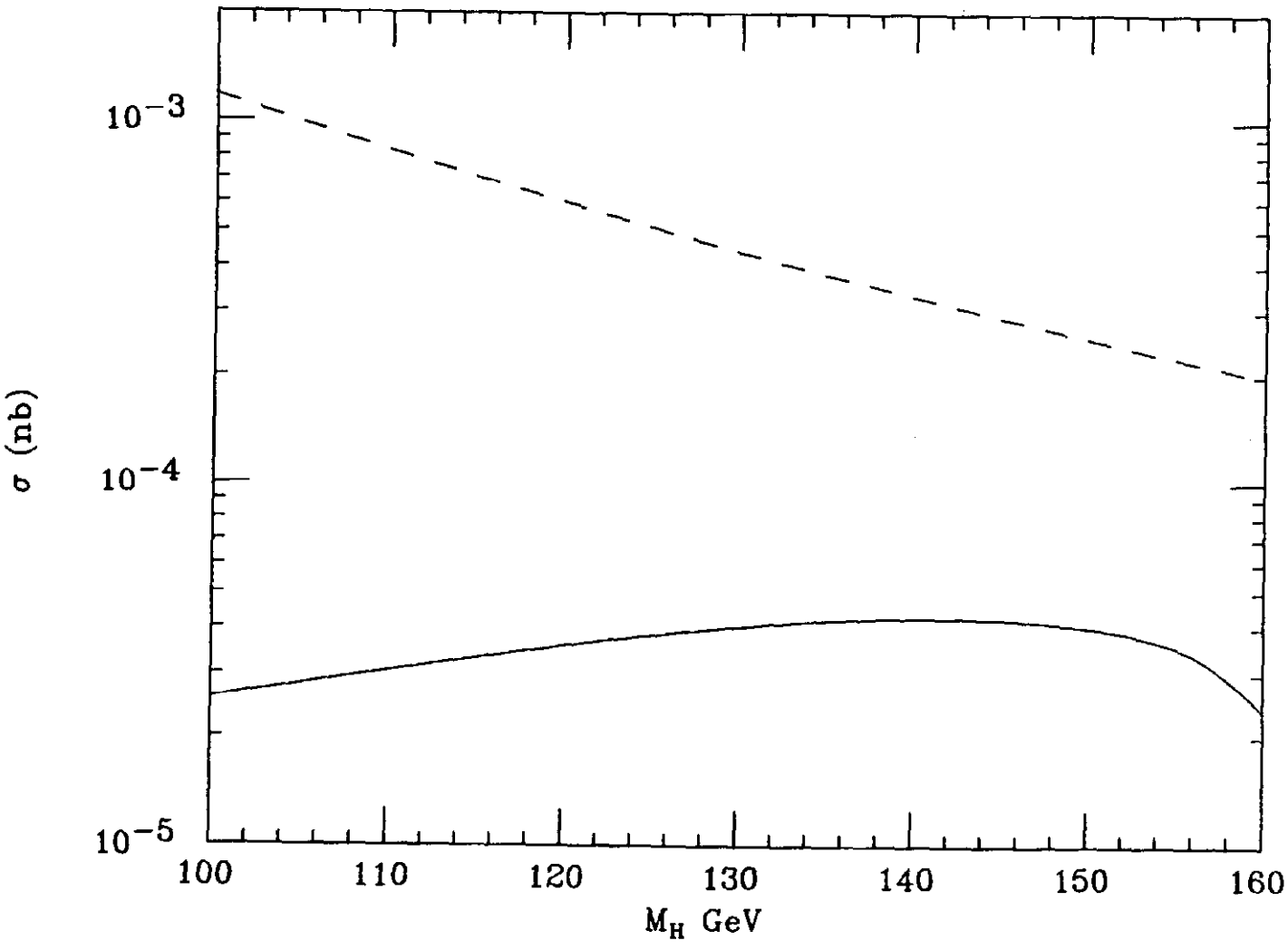

Figure 13

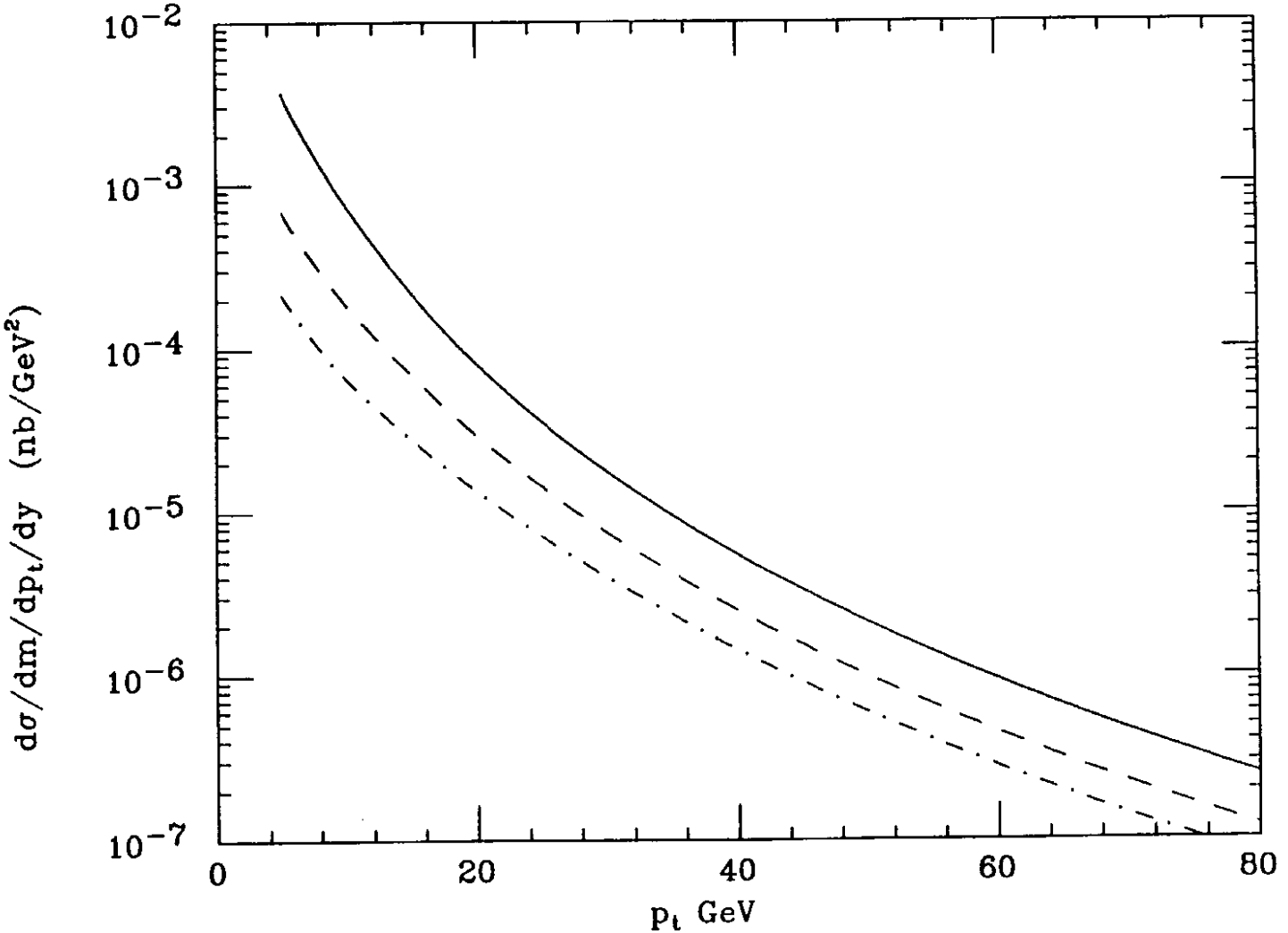
10^{-2}
10^{-3}
10^{-4}
10^{-5}
10^{-6}
10^{-7}
$d\sigma/dm/dp_t/dy$ (nb/GeV^2)
0
20
40
60
80
p_t GeV